

The perturbative QCD factorization approach in high energy nuclear collisions

Ivan Vitev† §

† Los Alamos National Laboratory, Mail Stop H846, Los Alamos, NM 87545,
USA

Abstract.

I discuss the systematic modifications to the perturbative QCD factorization approach in high energy $\ell+A$, $p+A$ and $A+A$ reactions. These include transverse momentum diffusion manifest in the Cronin effect and a small increase in the dijet acoplanarity; nuclear size enhanced power corrections that lead to shadowing in deeply inelastic scattering and suppression of single and double inclusive hadron production at forward rapidity at RHIC but disappear as a function of the transverse momentum; inelastic attenuation of the jet cross sections or jet quenching that persists to much higher p_T .

PACS numbers: 12.39.St; 12.38.Mh; 12.38.Cy; 24.85.+p; 25.30.-c

Submitted to: *J. Phys. G: Nucl. Phys.*

1. Introduction

The interpretation [1, 2] of the copious experimental results from the past, present and future heavy ion programs necessitates a reliable theoretical framework for the calculation of a variety of moderate and large transverse momentum processes, $Q^2 \sim p_T^2 \gg \Lambda_{\text{QCD}}^2$, that can be systematically extended to incorporate corrections arising from the many body nuclear dynamics. Such theoretical framework is the perturbative QCD factorization approach [3], a direct generalization of the naive parton model [4]. According to the factorization theorem, the observable hadronic cross sections can be expressed as

$$\sigma_{\text{hadronic}} = \sigma_{\text{partonic}}(x_i, z_j; \mu_r; \mu_{f\,i}, \mu_{d\,j}) \otimes \left\{ \prod_i \phi_{i/h_i}(x_i, \mu_{f\,i}) \right\} \otimes \left\{ \prod_j D_{h_j/j}(z_j, \mu_{d\,j}) \right\}; \quad (1)$$

where \otimes denotes the standard convolution over the internal kinematic variables of the reaction. In Eq. (1) μ_r , $\mu_{f\,i}$ and $\mu_{d\,j}$ are the renormalization, factorization and fragmentation scales, respectively. $\phi_{i/h_i}(x_i, \mu_{f\,i})$ is the distribution function (PDF) of parton “ i ” in the hadron h_i and $D_{h_j/j}(z_j, \mu_{d\,j})$ is the fragmentation or decay

§ E-mail address: ivitev@lanl.gov

function (FF) of parton “ j ” into hadron h_j . Factorization not only separates the short- and long-distance QCD dynamics but implies universality of the PDFs and FFs and infrared safety of the hard scattering partonic cross sections. If the $k_T i$ and/or the $j_T i$ dependence of the PDFs, FFs and σ_{partonic} is kept explicit, one arrives at a k_T and/or j_T factorized form [5]. At present, limited statistics hampers any reliable extraction of such transverse degrees of freedom. Integrating $k_T i$ and $j_T i$ out leads to the most commonly employed double collinear limit of QCD.

Factorization has been discussed in detail for a limited number of processes. Explicit examples of some fundamental cross sections are given below to lowest order and leading twist. All scales are suppressed and the definitions of the kinematic variables can be found in [6]. These examples include:

- (i) Electron-positron annihilation into hadrons [7]:

$$\frac{d\sigma_h}{dxdy} = N_c \frac{\pi\alpha_{em}^2}{q^2} \sum_j Q_i^2 (1 + \cos^2 \theta_{\text{cm}}) D_{h_j/j}(z_j). \quad (2)$$

Here $x = 2p \cdot q/q^2$, $y = \frac{1}{2}(1 - \cos \theta_{\text{cm}})$ and Q_i is the fractional electric charge of (anti)quarks in units of e . For a discussion on the structure of the near-side correlation function from fragmentation in $e^+ + e^-$ annihilation see [8].

- (ii) Deeply inelastic lepton-hadron scattering (DIS) with the longitudinal and transverse structure functions:

$$F_T = \frac{1}{2} \sum_i Q_i^2 \phi_f(x), \quad F_L = 0. \quad (3)$$

In Eq. (3) $x = x_B = -q^2/2p \cdot q = Q^2/2m_N\nu$ with $\nu = E - E'$. Recently the nuclear enhanced high twist corrections to the DIS cross sections have been evaluated within the factorization approach [9, 10]. Similar results from final state multiple scattering have been found in [11].

- (iii) The Drell-Yan process [12]:

$$\frac{d\sigma_{l^+l^-}}{dq^2} = \sum_i \phi_{i/N}(x_a) \phi_{\bar{i}/N'}(x_b) \frac{4\pi\alpha_{em}^2 Q_i^2}{3N_c q^2} \delta(q^2 - (x_a p + x_b p')^2). \quad (4)$$

In Eqs. (2) and (4) $N_c = 3$ is the number of colors. The momentum fractions $x_a = p_a^+/P_a^+$ and $x_b = p_b^+/P_b^+$.

- (iv) Inclusive hadron production in $N + N$ collisions to leading power and leading power corrections [13]. The single and double inclusive distributions accessible to $\mathcal{O}(\alpha_s^2)$ at leading twist read [14]:

$$\begin{aligned} \frac{d\sigma_{NN}^{h_1}}{dy_1 d^2 p_{T_1}} &= \sum_{abcd} \int \frac{dz_1}{z_1^2} D_{h_1/c}(z_1) \int dx_a \frac{\phi_{a/N}(x_a)}{x_a} \left[\frac{1}{x_a S + U/z_1} \right] \\ &\times \frac{\alpha_s^2}{S} \frac{\phi_{b/N}(x_b)}{x_b} |\overline{M}_{ab \rightarrow cd}|^2, \end{aligned} \quad (5)$$

$$\begin{aligned} \frac{d\sigma_{NN}^{h_1 h_2}}{dy_1 dy_2 d^2 p_{T_1} d^2 p_{T_2}} &= \frac{\delta(\Delta\varphi - \pi)}{p_{T_1} p_{T_2}} \sum_{abcd} \int \frac{dz_1}{z_1} D_{h_1/c}(z_1) D_{h_2/d}(z_2) \frac{\phi_{a/N}(\bar{x}_a)}{\bar{x}_a} \\ &\times \frac{\alpha_s^2}{S^2} \frac{\phi_{b/N}(x_b)}{x_b} |\overline{M}_{ab \rightarrow cd}|^2. \end{aligned} \quad (6)$$

In Eqs. (5) and (6) S , T and U are the *hadronic* Mandelstam variables [14]. The dependence on the small momentum fraction x_b , relevant to forward rapidity studies at RHIC, is explicitly isolated.

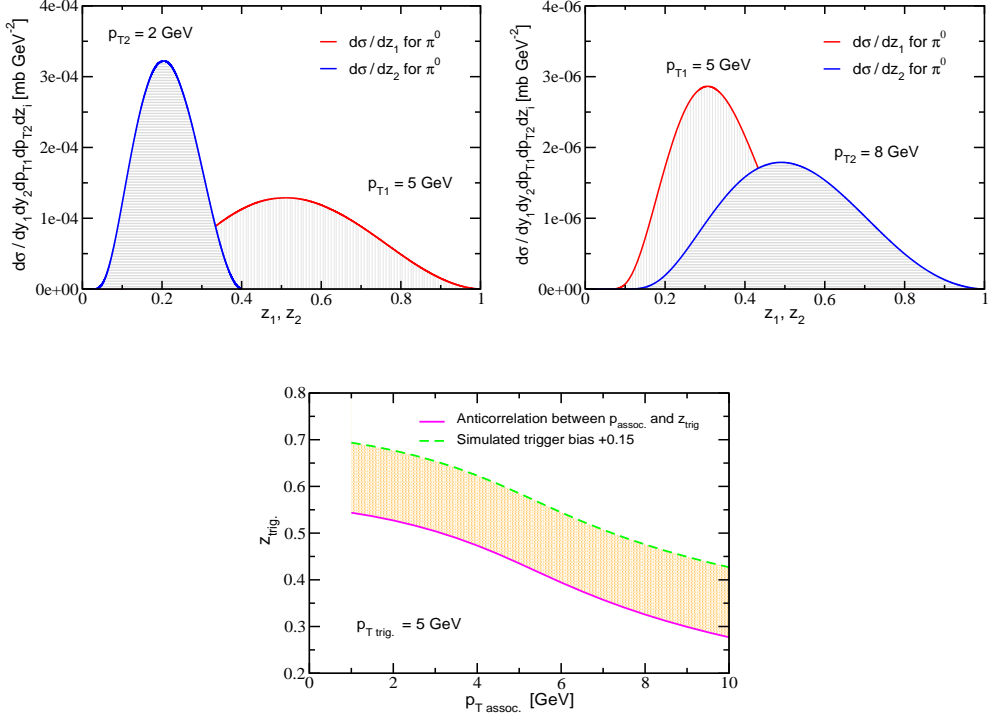


Figure 1. Left panel: the differential double inclusive π^0 distributions versus the fragmentation momentum fractions z_1, z_2 for a trigger pion of $p_T = 5 \text{ GeV}$ and associated pion of $p_T = 2 \text{ GeV}$. Right panel: the same cross sections for a trigger pion of $p_T = 5 \text{ GeV}$ and associated pion of $p_T = 8 \text{ GeV}$. Bottom panel: the anti-correlation between $z_{\text{trig.}}$ and $p_{T\text{assoc.}}$ for a fixed $p_{T\text{trig.}} = 5 \text{ GeV}$. The dashed line simulates a trigger bias $\Delta z_{\text{trig.}} = 0.15$.

(v) Heavy quark and heavy quark bound state production [15].

1.1. The fragmentation seesaw analogy

One of the exciting theoretical questions, prompted by the recent experimental results [16, 17], is about the nature of the hadron production mechanism at small and moderate p_T in $A + A$ reactions [18, 19, 20, 21]. The measurement of correlations [22] in $p + p$ and especially $d + Au$ collisions already provide sufficient evidence that back-to-back hard partonic scattering and fragmentation, Eqs. (5) and (6), give a dominant contribution to the particle cross sections. Corrections in the basic perturbative formulas arise both from higher orders in α_s and from higher twist. These may be enhanced by the nuclear size and the density of the quark-gluon plasma (QGP) in the deconfined phase. Such corrections can be systematically organized in the framework of the factorization approach as follows [24]:

$$\begin{aligned} \sigma_{\text{hadron}} &= \sigma_0^{(2)} \left(1 + C_1^{(2)} \alpha_s + C_2^{(2)} \alpha_s^2 + C_3^{(2)} \alpha_s^3 + \dots \right) T^{(2)} \\ &+ \frac{\sigma_0^{(4)}}{Q^2} \left(1 + C_1^{(2)} \alpha_s + C_2^{(2)} \alpha_s^2 + C_3^{(2)} \alpha_s^3 + \dots \right) T^{(4)} \end{aligned}$$

$$+ \frac{\sigma_0^{(6)}}{Q^4} \left(1 + C_1^{(2)} \alpha_s + C_2^{(2)} \alpha_s^2 + C_3^{(2)} \alpha_s^3 + \dots \right) T^{(6)} + \dots \quad (7)$$

In Eq. (7) $T^{(i)}$ are the twist “i” non-perturbative matrix elements. Odd-twist matrix elements play an important role in spin physics [25] but are here neglected for simplicity.

As a test of the dominance of the lowest order, leading twist term one can experimentally look for a seesaw fragmentation *analogy*. The seesaw mechanism [26] extends the Standard Model [27] by including a massive right-handed Majorana neutrino. The physical neutrino masses are given by $M_\nu = M_T M_R^{-1} M_T^\dagger$. When M_R is very large and hence ν_R is unobservable, M_ν can become very small.

Similar anti-correlation is present in Eq. (6). Naively, one might expect that a high- p_T hadron trigger in the near side will fix the fragmentation momentum fraction z_{trig} . In contrast, $\delta(p_{T1}/z_1 - p_{T2}/z_2)$ implies that z_{trig} is inversely proportional to p_T assoc . Figure 1 shows the differential distributions $d\sigma^{h_1 h_2}/dy_1 dy_2 dp_{T1} dp_{T2} dz_i$ for different choices of $p_{T\text{ trig}}$ and $p_{T\text{ assoc}}$. Experimental verification of the anti-correlation presented in the bottom panel of Fig. 1 can provide critical additional evidence in support of the dominance of the perturbative QCD hadron production mechanism and the cross section hierarchy summarized by Eq. (7).

2. Transverse momentum diffusion

Hard processes in the nuclear environment involve multiple parton interactions before or after the large Q^2 collision that are sensitive to the properties of the nuclear matter. In this section we consider the multiple elastic and incoherent scattering of energetic quarks and gluons that penetrate hot and cold QCD matter. Traverse momentum diffusion reflects the $\langle p_T^2 \rangle$ -kick per unit length in the medium, given by the transport coefficient $\mu^2/\lambda_{q,g}$, and is the strong interaction dynamics equivalent of the Moliere multiple scattering in QED.

Approximate solutions for the parton broadening can be obtained to leading power and leading power corrections in the large “+” lightcone momentum p^+ [28]. For the instructive case of a normalized forward monochromatic beam ($p_0 = p_{\parallel} \equiv P$) the initial quark or gluon distribution reads:

$$\frac{d^3 N^i}{dp^+ d^2 \mathbf{p}_\perp} \Big|_{p^- = \frac{\mathbf{p}_\perp^2}{2p^+}} = \delta(p^+ - \sqrt{2}P) \delta^2(\mathbf{p}_\perp). \quad (8)$$

In Eq. (8) the constraint on the parton’s “-” lightcone component from the $p^2 = 0$ on-shell condition is also shown. In the small angle approximation, rescattering leads to an approximately Gaussian form [28]:

$$\frac{d^3 N^f(p^+, \mathbf{p}_\perp)}{dp^+ d^2 \mathbf{p}_\perp} \Big|_{p^- = \frac{\mathbf{p}_\perp^2}{2p^+}} = \frac{1}{2\pi} \frac{e^{-\frac{\mathbf{p}_\perp^2}{2\chi\mu^2\xi}}}{\chi\mu^2\xi} \delta \left[p^+ - \left(\sqrt{2}P - \frac{1}{\sqrt{2}} \frac{\chi\mu^2\xi}{2P} \right) \right], \quad (9)$$

where $\chi = L/\lambda$ is the opacity or mean number of scatterings and $\xi = \mathcal{O}(1)$. It should be realized that this form is not expected to describe well the large angle scattering. The tails of the large \mathbf{p}_\perp distributions are expected to be power-law like and die out at a much slower rate than the Gaussian in Eq. (9). This may lead to uncertainties in the separation of the jet and the underlying event [22].

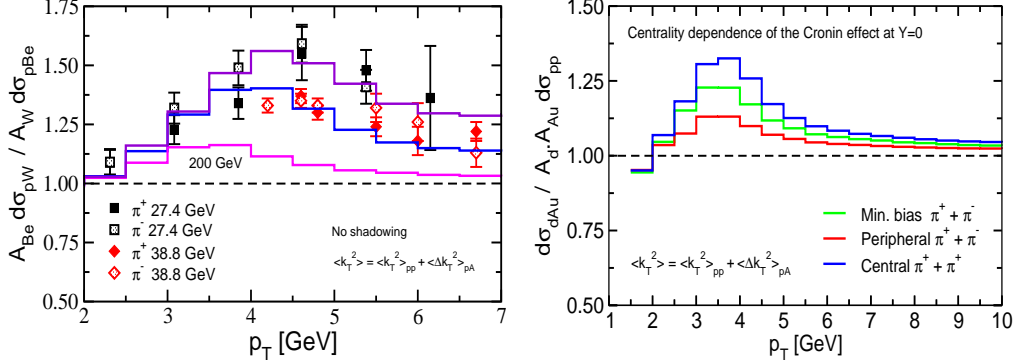


Figure 2. Left panel from [31]: calculation of the Cronin effect for $\pi^+ + \pi^-$ at $\sqrt{s_{NN}} = 27.4$ and 38.8 GeV at midrapidity. The nuclear modification is identified from the ratio of the cross sections in $p + W$ and $p + Be$ reactions. Right panel from [31]: predicted magnitude and centrality dependence of $R_{dA}^{(1)}(\mathbf{p}_T)$ at $\sqrt{s_{NN}} = 200$ GeV and midrapidity at RHIC in the absence of significant antishadowing.

2.1. Applications of transverse momentum diffusion

From Eq. (9) it is easy to demonstrate that the the accumulated acoplanarity momentum squared by an energetic parton probes a line integral through the color charge density:

$$\langle \Delta \mathbf{k}_T^2 \rangle \approx 2\xi \int dz \frac{\mu^2}{\lambda_{q,g}} = 2\xi \int dz \frac{3C_R \pi \alpha_s^2}{2} \rho^g(z) \\ = \begin{cases} 2\xi \frac{3C_R \pi \alpha_s^2}{2} \rho^g \langle L \rangle, & \text{static} \\ 2\xi \frac{3C_R \pi \alpha_s^2}{2} \frac{1}{A_\perp} \frac{dN^g}{dy} \ln \frac{\langle L \rangle}{\tau_0}, & 1+1D \end{cases} \quad (10)$$

In Eq. (10) the factor 2 comes from 2D diffusion, and ρ^g is the effective gluon density. For the 1+1D Bjorken expansion scenario A_\perp is the transverse area of the interaction region, τ_0 is the initial equilibration time and dN^g/dy is the effective gluon rapidity density.

Dynamical nuclear-induced modification in multi-particle production can be studied through the ratio [14]:

$$R_{AB}^{(n)} = \frac{d\sigma_{AB}^{h_1 \dots h_n} / dy_1 \dots dy_n d^2 p_{T_1} \dots d^2 p_{T_n}}{\langle N_{AB}^{\text{coll}} \rangle d\sigma_{NN}^{h_1 \dots h_n} / dy_1 \dots dy_n d^2 p_{T_1} \dots d^2 p_{T_n}}. \quad (11)$$

Centrality dependence is implicit in Eq. (11). The first and possibly most sensitive indicator of multi-parton dynamics in cold nuclear matter is the Cronin effect [29] in the single inclusive hadron production in $p + A$ reactions, $R_{pA}^{(1)}(\mathbf{p}_T)$.

Elastic transverse momentum diffusion at midrapidity is manifest in the Cronin enhancement at $p_T \geq 1 - 2$ GeV and suppression for $p_T \leq 1 - 2$ GeV. For a survey of theoretical models see [30]. Calculations of the nuclear modification in low energy $p + A$ reactions employ $\mu^2/\lambda = 0.1 - 0.14$ GeV² and are shown in the left hand side of Fig. 2. The predicted [31] centrality dependence of the Cronin effect in $d + Au$

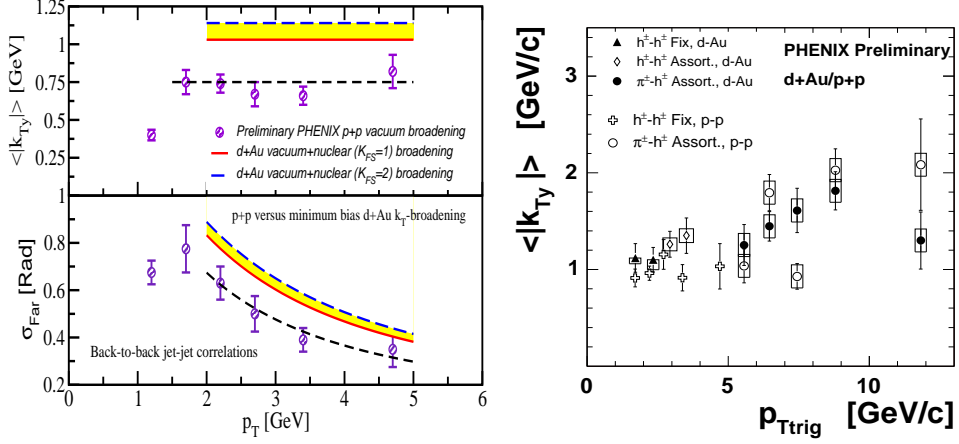


Figure 3. Left panel from [28]: the acoplanarity momentum projection per parton $\langle |k_T y| \rangle$ and the corresponding width σ_{Far} of the away-side correlation function for $p + p$ and $d + Au$. The approximations of $z_{\text{trig}} \rightarrow 1$ and constant $\langle |k_T y| \rangle_{pp} = 0.75$ had been used. Right panel from [22]: preliminary PHENIX data on the vacuum and medium induced acoplanarity momentum projection per parton in cold nuclear matter for realistic finite z_{trig} . Note the absence of significant difference between the $p + p$ and $d + Au$ measurements.

reactions at $y = 0$ and RHIC $\sqrt{s_{NN}} = 200$ GeV is given in the right hand side of Fig. 2 and confirmed by experimental data [22, 23, 32]. It is important to emphasize that even a small broadening may lead to a noticeable Cronin effect since it is amplified by the steepness of the partonic/hadronic spectra.

It is interesting to look for other manifestations of transverse momentum diffusion such as increased dijet acoplanarity, which will be reflected in the increased width of the away-side correlation function

$$C_2(\Delta\varphi) = \frac{1}{N_{\text{trig}}} \frac{dN_{\text{dijet}}^{h_1 h_2}}{d\Delta\varphi} \approx \frac{A_{\text{Near}}}{\sqrt{2\pi}\sigma_{\text{Near}}} e^{-\frac{\Delta\varphi^2}{2\sigma_{\text{Near}}^2}} + \frac{A_{\text{Far}}}{\sqrt{2\pi}\sigma_{\text{Far}}} e^{-\frac{(\Delta\varphi-\pi)^2}{2\sigma_{\text{Far}}^2}}. \quad (12)$$

In Eq. (12) the near-side width σ_{Near} of $C_2(\Delta\varphi)$ is determined by jet fragmentation and σ_{Far} reflects $\langle \mathbf{k}_T^2 \rangle_{\text{tot}} = \langle \mathbf{k}_T^2 \rangle_{pp} + \langle \mathbf{k}_T^2 \rangle_{nucl.}$.

The left panel of Fig. 3 shows the upper limit of the medium induced acoplanarity relative to the vacuum $p+p$ result. The predicted increase in the width of the away-side correlation function is small even in the $z_{\text{trig}} \rightarrow 1$ limit. For realistic fragmentation momentum fractions, see Fig. 1, the experimentally observed enhancement of $\langle \Delta\mathbf{k}_T^2 \rangle_{\text{tot}}$ should be significantly smaller. In addition, for dihadron angular correlations there are no amplification effects from the steepness of the underlying parton spectra. The right panel of Fig. 3 indeed shows the lack of significant difference between $p + p$ and $d + Au$ measurements and certainly excludes monojet-based models.

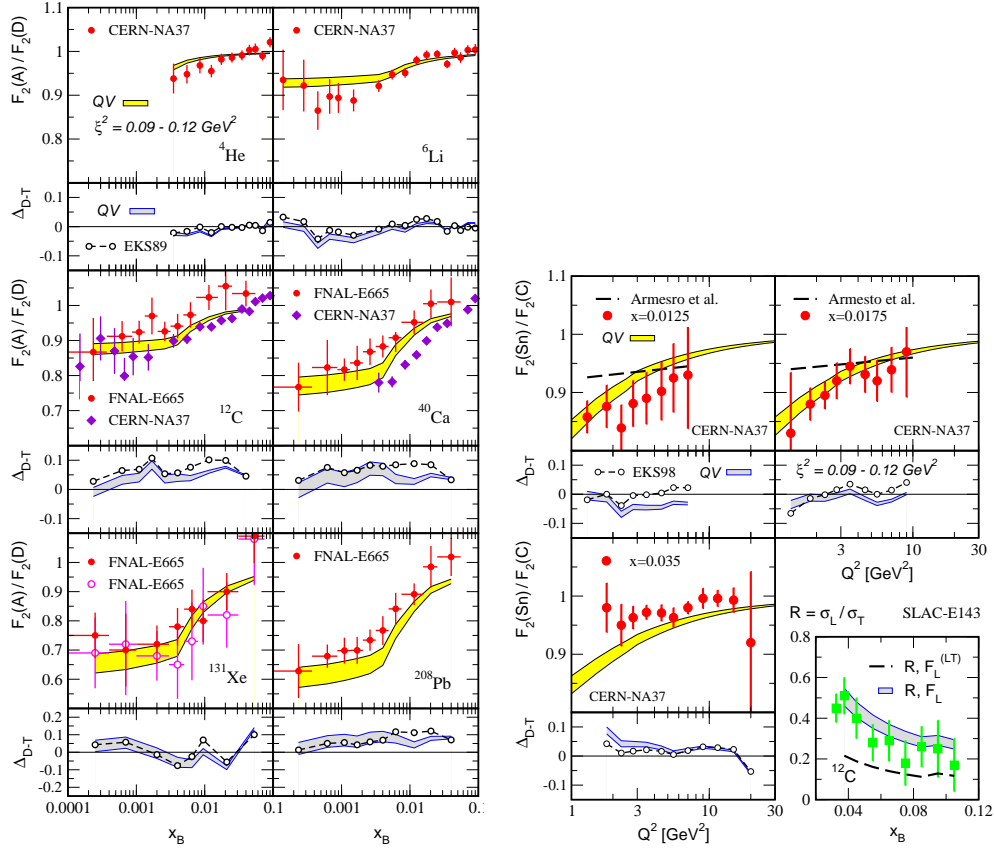


Figure 4. Left panel from [9]: all-twist resummed $F_2(A)/F_2(D)$ calculation from versus CERN-NA37 and FNAL-E665 data on DIS on nuclei. The band corresponds to the choice $\xi^2 = 0.09 - 0.12 \text{ GeV}^2$. Data-Theory, where Δ_{D-T} is computed for the set presented by circles, also shows comparison to the EKS98 scale-dependent shadowing parametrization. Right panel from [9]: CERN-NA37 data on $F_2(Sn)/F_2(C)$ show evidence for a power-law in $1/Q^2$ behavior consistent with the all-twist resummed calculation. The bottom right insert illustrates the role of higher twist contributions to F_L on the example of $R = \sigma_L/\sigma_T$.

3. Nuclear enhanced power corrections

A class of corrections that can be naturally incorporated in the perturbative QCD factorization approach is associated with the power suppressed $\sim 1/Q^n$, $n \geq 1$ contributions. The higher twist terms in Eq. (7) are typically neglected in reactions with “elementary” nucleons for $Q^2 \geq 1 \text{ GeV}^2$. However, in the presence of nuclear matter such corrections can be enhanced by the large nuclear size $\sim A^{1/3}$. These lead to dynamical nuclear shadowing. We discuss this mechanism in detail below.

Hard scattering in nuclear collisions requires one large momentum transfer $Q \sim xP \gg \Lambda_{QCD}$ with parton momentum fraction x and beam momentum P . A simple example is the lepton-nucleus deeply inelastic scattering (DIS). The transverse area probed by the virtual meson $\sim 1/Q^2$ is very small for moderate and large Q^2 processes. Hence, the struck quark will propagate in the nucleus and interact with nucleons along

the same impact parameter. If $Q^2 \ll m_N^2$ the *transverse* size of the wave packet will be comparable or larger than the size of the nucleon. In this case the rapid fall-off of the parton wave function effectively limits $Q^2 \geq Q_0^2$. The effective longitudinal interaction length probed by the virtual meson of momentum q^μ is characterized by $1/xP$. If the momentum fraction of an active initial-state parton $x \ll x_c = 1/2m_N r_0 \sim 0.1$ with nucleon mass m_N and radius r_0 , it could cover several Lorentz contracted nucleons of longitudinal size $\sim 2r_0(m_N/P)$ in a large nucleus.

Each of the multiple soft interactions is characterized by a scale of power correction per nucleon

$$\xi^2 \approx \frac{3\pi\alpha_s(Q)}{8r_0^2} \langle p | \hat{F}^2 | p \rangle, \quad (13)$$

with the matrix element $\langle p | \hat{F}^2 | p \rangle = \frac{1}{2} \lim_{x \rightarrow 0} xG(x, Q^2)$. A large nucleus will provide $\sim A^{1/3}$ enhancement of the high twist shadowing contribution. We note the Eq. (13) has the geometric average for minimum bias reactions incorporated in the definition of ξ^2 .

3.1. Applications of dynamical power corrections

In Ref. [9] we resummed the nuclear enhanced high twist corrections and identified the modification to the leading twist and lowest non-vanishing order in α_s contribution to the longitudinal and transverse structure functions:

$$F_T^A(x, Q^2) \approx A F_T^{(\text{LT})} \left(x + \frac{x\xi^2(A^{1/3} - 1)}{Q^2}, Q^2 \right), \quad (14)$$

$$F_L^A(x, Q^2) \approx A F_L^{(\text{LT})}(x, Q^2) + \frac{4\xi^2}{Q^2} F_T^A(x, Q^2). \quad (15)$$

These results, when compared to Eq. (3), indicate that the essential difference from the final state coherent multiple parton scattering is the generation of dynamical mass and the consequent rescaling in the value of Bjorken- x . In addition, there is a novel contribution to F_L^A .

Calculations of nuclear shadowing versus x_B with $\xi^2 = 0.09 - 0.12 \text{ GeV}^2$ are given in left panel of Fig. 4. The right panel shows the Q^2 dependence of power corrections and the enhancement in the longitudinal structure function, see Eq. (15), reflected in $R = \sigma_L/\sigma_T$.

This resummation, derived within the framework of the pQCD factorization approach [9] has definite advantages:

- It relies on standard PDFs [33] and its particularly easy to implement numerically. The final state soft scattering of the struck parton in the medium generates dynamical parton mass $m_{\text{dyn}}^2 = \xi^2(A^{1/3} - 1)$ via the coupling to the background chromo-magnetic field given by the two gluon correlation function, Eq. (13). The necessary additional energy leads to the rescaling of the value of Bjorken- x . This physical interpretation becomes transparent when we examine the behavior of $\nu + A$ DIS with charged current exchange and charm quark in the final state [10] with large physical mass M_c . Such processes are allowed via the CKM matrix mixing and we find:

$$x_B \rightarrow x_B + x_B \frac{M_c^2}{Q^2} + x_B \frac{\xi^2(A^{1/3} - 1)}{Q^2} = x_B \left(1 + \frac{M_c^2 + m_{\text{dyn}}^2}{Q^2} \right). \quad (16)$$

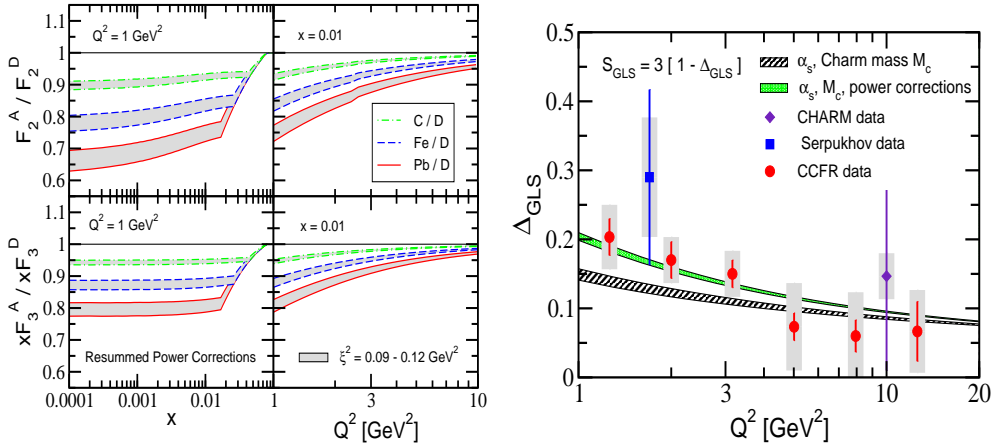


Figure 5. Left panel from [10]: predicted nuclear modification for isoscalar-corrected ^{12}C , ^{56}Fe and ^{208}Pb to the neutrino-nucleus DIS structure functions $F_2^A(x_B, Q^2)$ (top) and $x_B F_3^A(x_B, Q^2)$ (bottom) versus Bjorken x_B (left) and Q^2 (right). The bands correspond to $\xi^2 = 0.09 - 0.12 \text{ GeV}^2$. Right panel from [10]: Δ_{GLS} calculated to $\mathcal{O}(\alpha_s)$ with charm mass ($M_c = 1.35 \text{ GeV}$) effects (stripes) and $M_c + \text{resummed power corrections}$ (band). Data is from CCFR, CHARM and IHEP-JINR.

Similar rescaling of Bjorken- x has been derived in [34] for the EMC effect.

- This resummation provides a *natural framework* to understand the *differences* in the nuclear shadowing of sea quarks, valence quarks and gluons. In the leading-order and leading twist parton model in $\nu + A$ DIS $F_3^A(x_B, Q^2)$ measures the valance quark number density with $\phi_{\text{val.}}(x) \propto x^{-\alpha_{\text{val.}}}$ at small x . $F_2^A(x_B, Q^2)$, a singlet distribution, is proportional to the momentum density of all interacting quark constituents and for $x_B \ll 0.1$ is dominated by the sea contribution, $\phi_{\text{sea}}(x) \propto x^{-\alpha_{\text{sea}}}$. Therefore, the x_B -dependent shift from dynamical nuclear enhanced power corrections, Eq. (16), generates different modification to $F_2^A(x_B, Q^2)$ and $F_3^A(x_B, Q^2)$. Predictions for the x_B - and Q^2 -dependence of shadowing in $\nu + A$ reactions is given in the left panel of Fig. 5. The right panel shows the high-twist contribution to the Gross-Llewellyn Smith QCD sum rule [35]:

$$S_{\text{GLS}} = 3(1 - \Delta_{\text{GLS}}) = \int_0^1 dx_B \frac{1}{2x_B} \left(x_B F_3^{(\nu A)} + x_B F_3^{(\bar{\nu} A)} \right). \quad (17)$$

- Gluon shadowing is also easily understood within the same resummation approach as the final state scattering of the struck gluon [14] in $p + A$ reactions. In the color singlet approximation gluons couple twice as strongly to the medium in comparison to quarks. The scale of power corrections then reads $(C_A/C_F)\xi^2 = 2.25\xi^2 = 0.20 - 0.27 \text{ GeV}^2$ and the corresponding dynamically generated gluon mass is twice as large.

We now focus on the effects of dynamical nuclear shadowing on forward rapidity hadron production at RHIC. Any attenuation of the perturbative cross sections from coherent or inelastic parton scattering can be detected through the nuclear modification ratio $R_{AB}^{(n)}$, Eq. (11). In the special case of dihadron correlations such cross section reduction will be manifest in the attenuation of

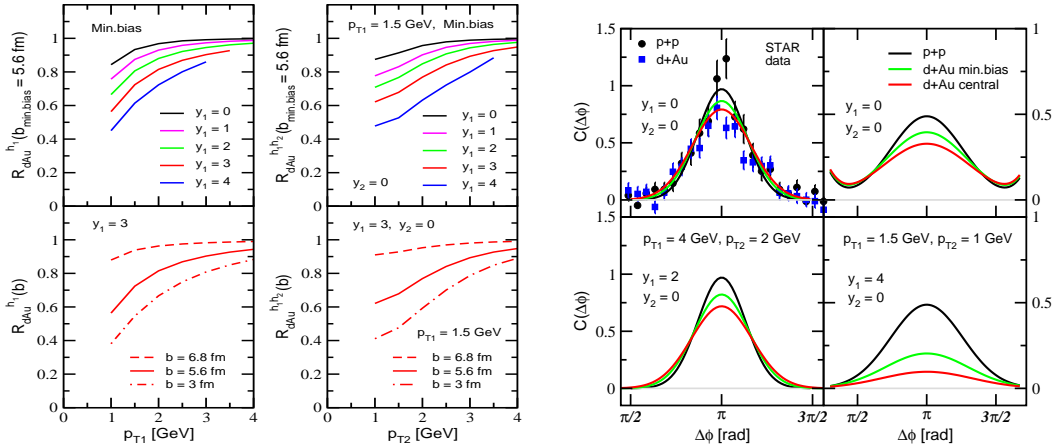


Figure 6. Left panel from [14]: suppression of the single and double inclusive hadron production rates in d+Au reactions versus p_T for rapidities $y_1 = 0, 1, 2, 3$ and 4. $\xi^2 = 0.12 \text{ GeV}^2$. Also shown is the impact parameter dependence of the calculated nuclear modification for central $b = 3 \text{ fm}$, minimum bias $b_{\text{min.bias}} = 5.6 \text{ fm}$ and peripheral $b = 6.9 \text{ fm}$ collisions. The trigger hadron $p_{T1} = 1.5 \text{ GeV}$, $y_1 = 3$ and the associated hadron $y_2 = 0$. Right panel from [14]: centrality dependence of $C_2(\Delta\varphi)$ at moderate $p_{T1} = 4 \text{ GeV}$, $p_{T2} = 2 \text{ GeV}$ and rapidities $y_1 = 0, 2$ and $y_2 = 0$. Central d+Au and p+p data from STAR. Also shown is $C_2(\Delta\varphi)$ at small transverse momenta $p_{T1} = 1.5 \text{ GeV}$, $p_{T2} = 1 \text{ GeV}$ and rapidities $y_1 = 0, 4$ and $y_2 = 0$.

the area A_{far} of the correlation function $C_2(\Delta\phi)$. In order to compute the process dependent nuclear shadowing we isolate the small x_b dependence of single and double inclusive hadron production, Eqs. (5) and (6),

$$F_{ab \rightarrow cd}(x_b) = \frac{\phi_{b/N}(x_b)}{x_b} |\overline{M}_{ab \rightarrow cd}|^2. \quad (18)$$

The final state interactions of the struck parton lead to rescaling of the small momentum fraction x_b as follows [14]:

$$F_{ab \rightarrow cd}(x_b) \Rightarrow F_{ab \rightarrow cd} \left(x_b \left[1 + C_d \frac{\xi^2}{-t} (A^{1/3} - 1) \right] \right). \quad (19)$$

In Eq. (19) C_d keeps track of the representation of the struck parton with $C_d = 1$ for quarks and $C_d = 2.25$ for gluon, as discussed above.

Figure 6 show the predicted suppression of the single and double inclusive differential hadron production cross sections versus rapidity and centrality. The scale of power corrections was extracted for minimum bias collisions and the impact parameter dependence can be obtained via the corresponding rescaling with the nuclear thickness function. It is important to note that the value of ξ^2 remains *unchanged*. However, in going from midrapidity to forward rapidity the perturbative scale $-t$ that enters in Eq. (19) changes from $\sim 2p_T^2$ to $\sim p_T^2$. This trivial kinematic dependence, which leads to larger suppression at forward rapidity, has been neglected in previous calculations. The right panel of Fig. 6 shows the combined effect of the the small transverse momentum broadening and nuclear enhanced power corrections. In contrast to alternative hypotheses, the high-twist shadowing goes away quickly with the virtuality or transverse momentum as long as the large $x_a \rightarrow 1$ threshold effects remain unimportant [36].

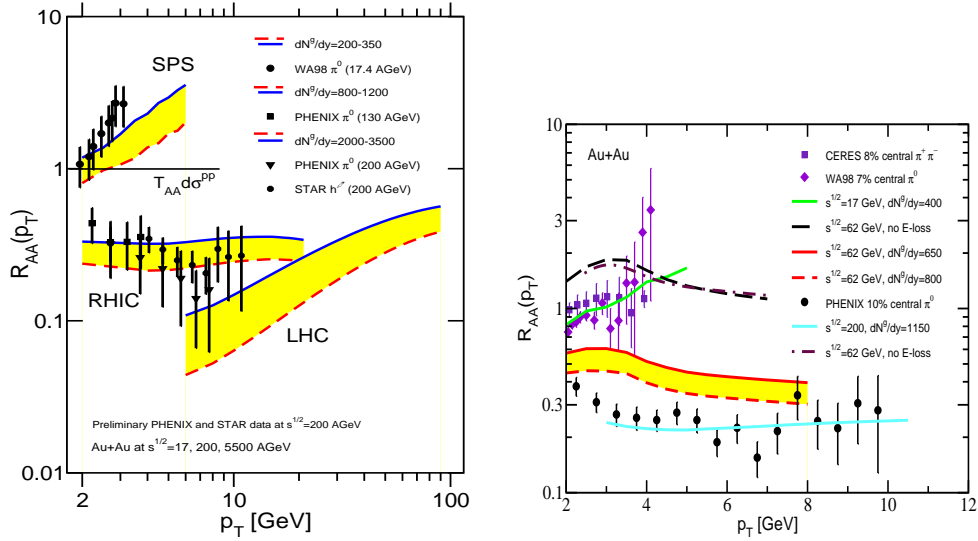


Figure 7. Left panel from [31]: suppression/enhancement ratio $R_{AA}(p_T)$ for neutral pions at $\sqrt{s}_{NN} = 17, 200, 5500$ GeV. Solid (dashed) lines correspond to the smaller (larger) effective initial gluon rapidity densities at given \sqrt{s} that drive parton energy loss. Right panel from [48]: predicted nuclear modification factor at $\sqrt{s}_{NN} = 62$ GeV for central $Au + Au$ collisions. Enhancement, arising from transverse momentum diffusion in cold nuclear matter without final state energy loss is given for comparison.

Further observations on the effects of nuclear shadowing on hadron production in $d + Au$ at RHIC is available in [37]. Preliminary study of the effects of higher-twist resummation [9, 10, 14] on the low Q^2 modification to the DGLAP evolution equations has recently become available [38].

4. Jet quenching and jet tomography

One of the few predicted [39] and observed signatures of nuclear dynamics associated with the presence of a hot and dense QCD plasma is the suppression of the high- p_T hadrons or jet quenching. While different attenuation mechanisms have been proposed [40], it is the multiple inelastic parton scattering in the final state that was able to quantitatively predict many of the hadronic observables associated with jet quenching [22, 23, 42]. Different approximations to the medium-induced non-Abelian gluon bremsstrahlung dynamics can be found in [43]. In this section we give details of the Reaction Operator approach [44], a momentum space iterative scheme for computing the radiation intensity.

The full solution for the medium induced gluon radiation off jets produced in a hard collisions at early times $\tau_{jet} \simeq 1/E$ inside a nuclear medium of length L can be obtained to all orders in the correlations between the multiple scattering centers in the GLV approach [44]. The double differential bremsstrahlung intensity for gluons with momentum $k = [xp^+, \mathbf{k}^2/xp^+, \mathbf{k}]$ resulting from the sequential interactions of a

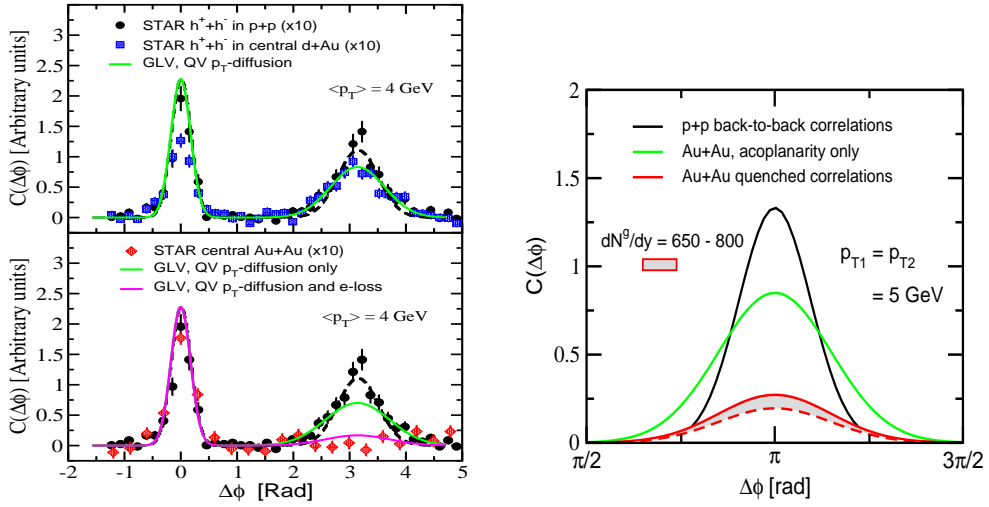


Figure 8. Left panel from [53]: the broadening of the away-side dihadron correlation function in central $d+Au$ and $Au+Au$ compared to scaled STAR data. In the bottom panel the broadening with and without suppression, $\propto R_{AA}$, is shown. Right panel from [48]: attenuation of the double inclusive pion production cross section for $p_{T1} = p_{T2} = 5$ GeV at intermediate RHIC energies.

fast parton with momentum $p = [p^+, 0, \mathbf{0}]$ can be written as:

$$\begin{aligned}
 x \frac{dN_g}{dx d^2\mathbf{k}} &= \sum_{n=1}^{\infty} x \frac{dN_g^{(n)}}{dx d^2\mathbf{k}} = \sum_{n=1}^{\infty} \frac{C_R \alpha_s}{\pi^2} \prod_{i=1}^n \int_0^{L - \sum_{a=1}^{i-1} \Delta z_a} \frac{d\Delta z_i}{\lambda_g(i)} \\
 &\times \int d^2\mathbf{q}_i \left[\sigma_{el}^{-1}(i) \frac{d\sigma_{el}(i)}{d^2\mathbf{q}_i} - \delta^2(\mathbf{q}_i) \right] \left(-2 \mathbf{C}_{(1, \dots, n)} \cdot \sum_{m=1}^n \mathbf{B}_{(m+1, \dots, n)(m, \dots, n)} \right. \\
 &\times \left. \left[\cos \left(\sum_{k=2}^m \omega_{(k, \dots, n)} \Delta z_k \right) - \cos \left(\sum_{k=1}^m \omega_{(k, \dots, n)} \Delta z_k \right) \right] \right), \quad (20)
 \end{aligned}$$

where $\sum_2^1 \equiv 0$ is understood. In the small angle eikonal limit $x = k^+/p^+ \approx \omega/E$. In Eq. (20) the color current propagators, the formation times and the elastic scattering cross section are defined in [44]. For a derivation in the case of heavy quarks see [45].

Qualitatively, the behavior of the energy loss as a function of the density and the size of the system can be summarized to first order in opacity as follows:

$$\begin{aligned}
 \langle \Delta E \rangle &\approx \int dz \frac{C_R \alpha_s}{2} \frac{\mu^2}{\lambda_g} z \ln \frac{2E}{\mu^2 \langle L \rangle} = \int dz \frac{9C_R \pi \alpha_s^3}{4} \rho^g(z) \ln \frac{2E}{\mu^2 \langle L \rangle} \\
 &= \begin{cases} \frac{9C_R \pi \alpha_s^3}{8} \rho^g \langle L \rangle^2 \ln \frac{2E}{\mu^2 \langle L \rangle}, & \text{static} \\ \frac{9C_R \pi \alpha_s^3}{4} \frac{1}{A_\perp} \frac{dN^g}{dy} \langle L \rangle \ln \frac{2E}{\mu^2 \langle L \rangle}, & 1+1D \end{cases}. \quad (21)
 \end{aligned}$$

For static systems $\langle \Delta E \rangle$ depends quadratically on the nuclear size. For the case of longitudinal Bjorken expansion this dependence is reduced to linear [47] but the energy loss is sensitive to the initial parton rapidity density dN^g/dy . Understanding the effective color charge density dependence of ΔE is the key to jet tomography [31].

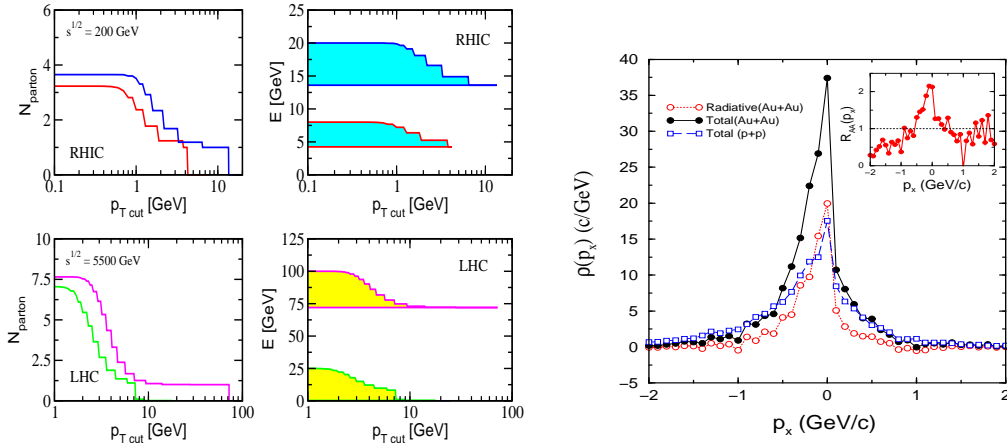


Figure 9. Left panel from [31]: induced partonic multiplicity as a function of the experimental p_T cut for energetic quark jets at RHIC and the LHC. Right panel from [54]: momentum density of hadrons associated with energetic back-to-back jets with and without medium induced bremsstrahlung. Secondary rescattering leads to gluon transverse momenta ~ 600 MeV.

Transverse expansion does not affect significantly the attenuation of the inclusive spectra [47].

4.1. Applications of jet quenching

The probability $P(\epsilon)$ for fractional energy loss $\epsilon = \sum_i \omega_i/E$ due to multiple gluon emission is evaluated in the independent Poisson approximation [46]. One way of implementing the parton momentum attenuation is via the kinematic rescaling of the momentum fraction $z_j \rightarrow z_j/(1-\epsilon)$ in the decay functions, Eq. (1). Consequently,

$$D_{h_j/j}(z_j, \mu_{d,j}) \rightarrow \int d\epsilon P(\epsilon) \frac{1}{1-\epsilon} D_{h_j/j} \left(\frac{z_j}{1-\epsilon}, \mu_{d,j} \right). \quad (22)$$

These corrections to the factorized formulas, Eqs. (5) and (6), can be easily implemented numerically.

The left panel of Fig. 7 shows the predicted nuclear modification [31] as a function of $\sqrt{s_{NN}}$ at SPS, RHIC and the LHC as a function of the density of the quark-gluon plasma. The p_T dependence of $R_{AA}^{(1)}$ is a result of the interplay of the Cronin effect, jet quenching and nuclear shadowing [49]. The right panel shows a theoretical estimate for the π^0 (or $\pi^+ + \pi^-$) attenuation at the intermediate RHIC energy of $\sqrt{s_{NN}} = 62$ GeV [48]. Such suppression is in agreement with the preliminary PHENIX and STAR measurements [23, 50] for $p_T > 3$ GeV. It is interesting to observe the better agreement between data and theory at the SPS with a recently extracted low energy $p + p$ baseline [51]. Similar suppression at the intermediate RHIC energy has been found in [52].

For double inclusive hadron production qualitatively $1 \leq R_{AA}^{h_1}/R_{AA}^{h_1 h_2} \leq 2$. This attenuation will be manifest as a reduction of the area A_{Far} of $C_2(\Delta\phi)$, Eq. (12). The left panel of Fig. 8 demonstrates that transverse momentum diffusion in $Au + Au$ collisions is insufficient to reproduce the disappearance of the away-side correlations [22]. Comparison to data require significant jet energy loss, compatible

with the attenuation in the single inclusions. The right panel shows the predicted quenching effect at $\sqrt{s_{NN}} = 62$ GeV [48].

The energy lost by the energetic partons during their propagation in dense nuclear matter is redistributed back in the partonic system. In the GLV approach [44] the medium induced virtuality is irradiated in higher frequency modes $\omega \geq \omega_{\text{pl}} \sim \mu$ resulting in fewer more energetic gluons. The left panel of Fig. 9 shows the the recovered jet energy as a function of the experimental p_T^{cut} and the corresponding induced parton multiplicity $+ 1(\text{jet})$. If the secondary (bremsstrahlung) gluons reinteract in the system [54] their momentum is further degraded to $p_T \simeq 600$ MeV and

$$N_g(\mathbf{r}, \Delta\tau) \approx \frac{1}{4} \Delta S = \frac{1}{4} \frac{\Delta E(\mathbf{r}, \Delta\tau)}{T(\mathbf{r}, \tau)} . \quad (23)$$

Numerical results for this scenario are shown in the right hand side of Fig. 9. For preliminary results on the recovery of the lost energy in jet measurements see [22, 55].

5. Conclusions

The predictive power of perturbative QCD is based one the factorization approach that has been successfully tested in a variety of moderate and high transverse momentum processes [3, 5, 7, 12, 13, 15] in elementary $N + N$ collisions. In this talk I discussed the theoretical and phenomenological aspects of the systematic incorporation of nuclear enhanced higher order and higher twist corrections in this formalism in $\ell + A$, $p + A$ and $A + A$ reactions. The current data on relativistic heavy ion reactions and the extended kinematic reach that is expected to become available due to improved statistics, RHIC upgrades, RHIC II and the LHC will help to further quantify the relative importance of the elastic [28, 30], inelastic [43, 44] and coherent [9, 10, 14] multiple parton scattering in cold and hot nuclear matter.

Acknowledgments: I would like to thank Mikkel Johnson for useful discussion. This work is supported by the J.R. Oppenheimer Fellowship of the Los Alamos National Laboratory and by the US Department of Energy.

References

- [1] BRAHMS Collaboration; PHENIX Collaboration; PHOBOS Collaboration, STAR Collaboration; White papers, to be published.
- [2] M. Gyulassy and L. McLerran, nucl-th/0405013; X. N. Wang, nucl-th/0405017; B. Muller, nucl-th/0404015; E. V. Shuryak, hep-ph/0405066; J. P. Blaizot and F. Gelis, hep-ph/0405305.
- [3] J. C. Collins, D. E. Soper and G. Sterman, Adv. Ser. Direct. High Energy Phys. **5** (1988) 1; Nucl. Phys. B **308**, 833 (1988).
- [4] J. D. Bjorken and E. A. Paschos, Phys. Rev. **185**, 1975 (1969); R. P. Feynman, Phys. Rev. Lett. **23**, 1415 (1969).
- [5] J. C. Collins and D. E. Soper, Nucl. Phys. B **194**, 445 (1982).
- [6] R. Brock *et al.*, Rev. Mod. Phys. **67**, 157 (1995).
- [7] J. C. Collins and D. E. Soper, Nucl. Phys. B **193**, 381 (1981) [Erratum-ibid. B **213**, 545 (1983)].
- [8] A. Majumder and X. N. Wang, hep-ph/0402245; A. Majumder, these proceedings.
- [9] J. W. Qiu and I. Vitev, hep-ph/0309094.
- [10] J. W. Qiu and I. Vitev, Phys. Lett. B **587**, 52 (2004).
- [11] S. J. Brodsky and H. J. Lu, Phys. Rev. Lett. **64**, 1342 (1990).
- [12] G. T. Bodwin, Phys. Rev. D **31**, 2616 (1985); J. C. Collins, D. E. Soper and G. Sterman, Nucl. Phys. B **261**, 104 (1985).
- [13] R. K. Ellis *et al.*, Phys. Lett. B **78**, 281 (1978); J. W. Qiu and G. Sterman, Nucl. Phys. B **353**, 137 (1991).

- [14] J. W. Qiu and I. Vitev, hep-ph/0405068.
- [15] G. T. Bodwin, E. Braaten and G. P. Lepage, Phys. Rev. D **51**, 1125 (1995) [Erratum-ibid. D **55**, 5853 (1997)].
- [16] K. Adcox *et al.*, Phys. Rev. Lett. **88**, 242301 (2002); C. Adler *et al.*, Phys. Rev. Lett. **89**, 092301 (2002).
- [17] T. Chujo, these proceedings; P.G. Jones, these proceedings.
- [18] L. V. Gribov, E. M. Levin and M. G. Ryskin, Phys. Rept. **100**, 1 (1983).
- [19] I. Vitev and M. Gyulassy, Phys. Rev. C **65**, 041902 (2002).
- [20] R. J. Fries, J. Phys. G **30**, S853 (2004), references therein; these proceedings; D. Molnar, these proceedings; C. Nonaka these proceedings; V. Greko, these proceedings.
- [21] T. Hirano, J. Phys. G **30**, S845 (2004), references therein; these proceedings; T. Renk, these proceedings.
- [22] C. Adler *et al.*, Phys. Rev. Lett. **90**, 082302 (2003); J. Adams *et al.*, Phys. Rev. Lett. **91**, 072304 (2003); K. Filimonov, J. Phys. G **30**, S919 (2004), references therein; these proceedings; J. Rak, J. Phys. G **30**, S1309 (2004), references therein; these proceedings; J. Jia, these proceedings; Y. Guo, these proceedings.
- [23] D. d'Enterria, J. Phys. G **30**, S767 (2004), references therein; these proceedings; J. L. Klay, these proceedings.
- [24] J. W. Qiu, hep-ph/0305161.
- [25] J. W. Qiu and G. Sterman, Phys. Rev. Lett. **67**, 2264 (1991); S. J. Brodsky, D. S. Hwang and I. Schmidt, Phys. Lett. B **530**, 99 (2002).
- [26] R. Slansky, Phys. Rept. **79**, 1 (1981).
- [27] S. Weinberg, Phys. Rev. Lett. **19**, 1264 (1967).
- [28] J. W. Qiu and I. Vitev, Phys. Lett. B **570**, 161 (2003); M. Gyulassy, P. Levai and I. Vitev, Phys. Rev. D **66**, 014005 (2002).
- [29] J. W. Cronin *et al.*, Phys. Rev. D **11**, 3105 (1975).
- [30] A. Accardi, hep-ph/0212148; references therein.
- [31] I. Vitev and M. Gyulassy, Phys. Rev. Lett. **89**, 252301 (2002); I. Vitev, Phys. Lett. B **562**, 36 (2003); J. Phys. G **30**, S791 (2004); references therein.
- [32] I. Arsene *et al.*, Phys. Rev. Lett. **91**, 072305 (2003); S. S. Adler *et al.*, Phys. Rev. Lett. **91**, 072303 (2003); B. B. Back, Phys. Rev. Lett. **91**, 072302 (2003).
- [33] J. Pumplin *et al.*, JHEP **0207**, 012 (2002); A. D. Martin, R. G. Roberts, W. J. Stirling and R. S. Thorne, Eur. Phys. J. C **23**, 73 (2002).
- [34] M. B. Johnson and J. Speth, Nucl. Phys. A **470** (1987) 488.
- [35] D. J. Gross and C. H. Llewellyn Smith, Nucl. Phys. B **14**, 337 (1969).
- [36] B. Kopeliovich, private communication; B. Kopeliovich, work in preparation.
- [37] R. Vogt, hep-ph/0405060; V. Guzey, M. Strikman and W. Vogelsang, hep-ph/0407201.
- [38] W. Zhu, hep-ph/0408328.
- [39] X. N. Wang and M. Gyulassy, Phys. Rev. Lett. **68**, 1480 (1992).
- [40] K. Gallmeister and W. Cassing, hep-ph/0408223;
- [41] W. Cassing, K. Gallmeister and C. Greiner, J. Phys. G **30**, S801 (2004), references therein.
- [42] S. Mioduszewski, nucl-ex/0409011; S. Mioduszewski, Nucl. Phys. A **715**, 199 (2003), references therein; these proceedings.
- [43] M. Gyulassy *et al.*, nucl-th/0302077; R. Baier, D. Schiff and B. G. Zakharov, Ann. Rev. Nucl. Part. Sci. **50**, 37 (2000).
- [44] M. Gyulassy, P. Levai and I. Vitev, Nucl. Phys. B **594**, 371 (2001); Phys. Rev. Lett. **85**, 5535 (2000); Nucl. Phys. B **571**, 197 (2000).
- [45] M. Djordjevic and M. Gyulassy, Nucl. Phys. A **733**, 265 (2004); Phys. Rev. C **68**, 034914 (2003); Phys. Lett. B **560**, 37 (2003).
- [46] R. Baier *et al.*, JHEP **0109**, 033 (2001); M. Gyulassy, P. Levai and I. Vitev, Phys. Lett. B **538**, 282 (2002).
- [47] M. Gyulassy, I. Vitev and X. N. Wang, Phys. Rev. Lett. **86**, 2537 (2001); M. Gyulassy *et al.*, Phys. Lett. B **526**, 301 (2002).
- [48] I. Vitev, nucl-th/0404052.
- [49] K. J. Eskola, V. J. Kolhinen and C. A. Salgado, Eur. Phys. J. C **9**, 61 (1999).
- [50] T. Awes, talk given at the 2004 AGS-RHIC users' meeting; Z. Xu, talk given at DPF 2004.
- [51] D. d'Enterria, Phys. Lett. B **596**, 32 (2004).
- [52] A. Adil and M. Gyulassy, nucl-th/0405036; X. N. Wang, Phys. Rev. C **70**, 031901 (2004).
- [53] I. Vitev, AIP Conf. Proc. **698**, 721 (2004); X. N. Wang, Phys. Lett. B **595**, 165 (2004).
- [54] S. Pal and S. Pratt, Phys. Lett. B **574**, 21 (2003).
- [55] F. Wang, J. Phys. G **30**, S1299 (2004).